Geocell-reinforced capping layer in rail tracks subjected to cyclic loading: laboratory and numerical modelling study

Trung Ngo, Ph.D., M.ASCE[1] and Buddhima Indraratna, Ph.D., F.ASCE[2]

[1]Senior lecturer, Transport Research Centre, School of Civil and Environmental Engineering, University of Technology Sydney, Ultimo, Australia (Corresponding author). ORCID: https://orcid.org/0000-0002-9676-3728. Email: Trung.Ngo@uts.edu.au
[2]Distinguished Professor of Civil Engineering and Director of Transport Research Centre, University of Technology Sydney, Ultimo, Australia. Email: buddhima.indraratna@uts.edu.au

ABSTRACT

This research investigates the behavior of geocell-reinforced capping layers in ballasted tracks subjected to cyclic loading. Large-scale laboratory testing and numerical modeling techniques were employed. The cyclic tests applied a 25-tonne axle load under frequencies ranging from 10 to 30 Hz. The geocell-reinforced capping layers were modeled using the Discrete Element Method The geocell structure was simulated by bonding small balls to build a realistic geometry and shape. Model parameters were calibrated based on tensile and bending tests performed on the geocell material. The DEM simulations accurately represented the irregular shape of the capping aggregates using bonded circular particles. The findings indicated that the geocell effectively reduced both vertical and lateral displacements of the capping layer. The DEM analysis provided valuable insights into the contact force chain distributions within the capping assembly.

INTRODUCTION

Railway tracks are essential elements of transportation infrastructure worldwide. Among the various types of tracks, ballasted railway tracks are widely utilized due to their cost-effectiveness and ease of maintenance (Selig and Waters, 1994). A crucial component of these tracks is the capping layer, which is positioned beneath the ballast and serves the important function of load transferring from the sleepers to the formation soils. Typically, the capping layer consists of coarse mixtures comprising naturally occurring or processed sand, gravel, or crushed aggregates (Esveld, 2014; Biabani et al., 2016, Banerjee et al. 2020). Its primary objectives are to minimize stress and prevent the subgrade from being infiltrated or mixed with the ballast material. Over time, due to repeated train loading, the capping aggregates tend to deteriorate and accumulate fine particles from external sources or experience upward movement of soft subgrade material, leading to fouling. These factors can considerably diminish the drainage capacity and shear strength of ballast (Indraratna and Ngo, 2018).

In recent years, polymer geosynthetic reinforcement, such as geocell, has been widely adopted to strengthen rail track substructures (Brown et al. 2007, Tutumluer et al. 2012, Luo et al. 2023). Past studies have indicated that geosynthetics have the ability to reinforce the ballast/capping layers, resulting in reduced vertical and lateral displacements of the track (Bathurst and Raymond 1987, Biabani et al. 2016). Geocell is a three-dimensional interconnected honeycomb structure that provides additional confinement to the capping layer, reducing track deformation (Leshchinsky and Ling 2013, Ngo et al. 2016, Astaraki et al. 2022). Due to its 3D structure, the geocell prevents the horizontal spreading of the in-fill aggregates and forms a stronger layer that distributes the load across a wider area.

Researchers have applied the discrete element method (DEM) to investigate various mechanical characteristics of ballast aggregates and granular materials (Cundall and Strack 1979, Bolton et al. 2008, Tran et al. 2013, McDowell and Li 2016, Bian et al. 2020). This approach enables the study of inter-particle movement, particle breakage, particle angularity, and contact force chains, which are difficult to investigate through experimental means. (Cui and O'Sullivan 2006, Zhang et al. 2019, Tran et al. 2020). While DEM has been utilized to study the mechanical properties of ballast aggregates, there has been limited research on the performance of geocell-reinforced capping. This study focuses on experimental tests and DEM simulations conducted on geocell-reinforced capping under cyclic train loading. To replicate real-world conditions, a track process simulation apparatus- TPSA was employed. The aim is to explore the response and behavior of the geocell-reinforced capping under cyclic loading, shedding light on its mechanical performance and interaction with the surrounding materials

TRACK PROCESS SIMULATION APPARATUS

A track process simulation apparatus, measuring 800 mm in length, 600 mm in width, and 450 mm in height was used to replicate a realistic ballasted rail track condition (Indraratna et al. 2017). The capping material, obtained from Bombo quarry in Australia, underwent cleaning and sieving to achieve a particle size distribution consistent with practices in New South Wales. The capping aggregates had a mean particle size of 3.3 mm. The experiments involved a 150-mm-high geocell with a cellular area of 46 x 103 mm2. The geocell was manufactured using polyethylene polymer strips and has a three-dimensional structure. The geocell has a bulk material tensile strength of 9.5 kN/m, while the welded sections had a tensile strength of 8.0 kN/m, as reported by Biabani et al. in 2016.

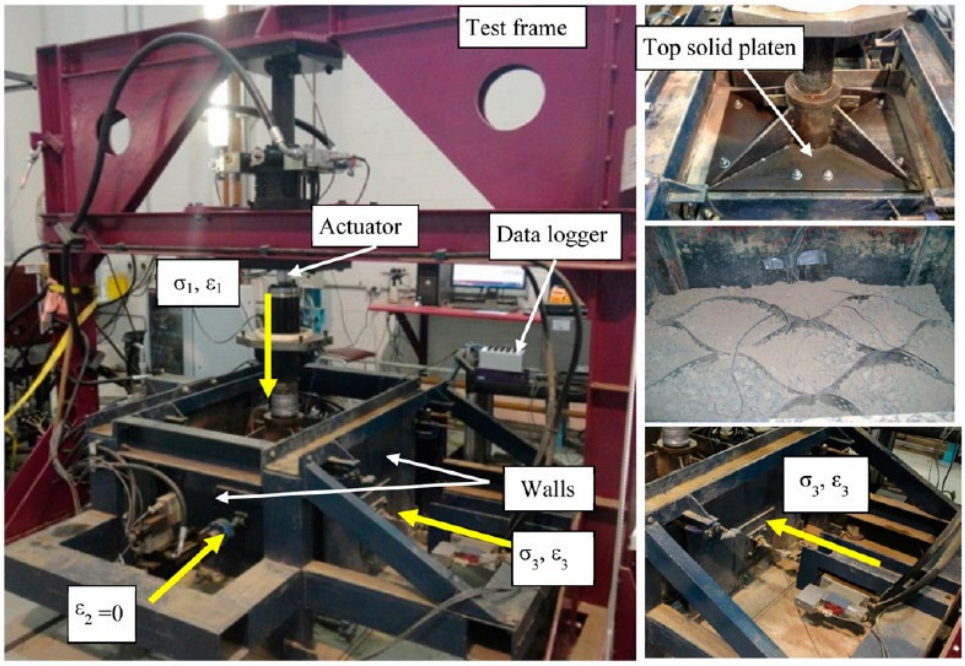

Figure 1. Track process simulation apparatus - TPSA (Source: Indraratna et al. 2015)

The capping aggregates were compacted in layers, with each layer having a thickness of 50mm. The total thickness of the compacted capping was 300mm, resulting in a density of 21kN/m^3 and a relative density of approximately 77%. Following the compaction of the capping, an 8-cell geocell was positioned on the top of the capping layer, as depicted in Figure 1. The remaining capping material was then compacted within each geocell compartment until the capping reached a thickness of 450mm.

To apply cyclic load, a hydraulic actuator was connected to a steel plate, thus transferring the load to the capping layer. A sinusoidal cyclic loading pattern was employed, with σ_{max} and σ_{min} of 166 kPa and 41 kPa, respectively, simulating the heavy haul train conditions with an axle load of approximately 25-30 tonnes. The stress and strain in a vertical direction are given as σ_1 and ε_1 while those in a transverse direction are given as σ_3 and ε_3. The strain in longitudinal direction was simulated as $\varepsilon_2=0$ (plane strain). The capping was subjected to testing with and without the inclusion of a geocell, while varying the confining pressures (ranging from 5 to 15 kPa) and frequencies, f (f= 10 to 30 Hz). The range of confining pressures aimed to replicate the effects of crib and shoulder ballast weight in real track scenarios. f=10Hz was chosen to represent the typical vibration frequency of freight trains traveling at around 75 km/h in New South Wales, Australia. Additionally, f=20 Hz, 30Hz were chosen to simulate higher vibration frequencies that might occur at higher train speeds of approximately 145-220 km/h.

DISCRETE ELEMENT MODELLING

A 2D discrete element modeling (DEM) approach was employed to investigate the interaction between geocell and capping. The DEM model, calibrated appropriately with laboratory test data, utilized a two-dimensional plane strain representation to simulate the behavior of the capping and geocell (Ngo et al. 2016). The longitudinal strain was considered negligible compared to the vertical and transverse strains. The geometry DEM model matched those of the physical TPSA used in the laboratory experiment. The vertical walls of the DEM model were divided into six parts, enabling independent horizontal movement of the capping in real track conditions (figure 2). This facilitated the capture of depth-dependent lateral displacement variations.

A servo-control facility was used to maintain the desired confining pressure (σ_3) on the left and right walls during the simulation. The bottom boundary was fixed to simulate the testing apparatus boundary. To mimic the realistic capping gradation, 26,567 particles with diameters ranging from 0.5 to 19 mm were randomly generated and oriented inside the model assembly (Figure 2). The particles had a representative density of the test. Sub-routines were programmed to replicate cyclic loading conditions similar to the laboratory tests, with σ_{max} and σ_{min} of 166 kPa and 41 kPa. The assembly was brought to equilibrium, ensuring the particles established contacts while maintaining a constant void ratio.

In discrete element modeling (DEM), the contact force between particles is determined by the force-displacement law, which considers the relative displacement between them. The contact force vector $\vec{F}$ is divided into normal component ($\vec{F}_N$) and shear component ($\vec{F}_T$), with respect to the contact plane:

$$\vec{F}_N = K_N \cdot U^n \tag{1}$$

$$\delta\vec{F}_T = -K_T \cdot \delta U^s \tag{2}$$

where, δU^s is the shear displacement incremental; $\delta\vec{F}_T$ is shear force the incremental; K_N and K_T are the shear and normal stiffnesses;

The computation of the normal contact stiffness for the linear contact model utilized in this study was performed as part of the analysis:

$$K_N = \frac{k_n^{[A]} k_n^{[B]}}{k_n^{[A]} + k_n^{[B]}} \tag{3}$$

Contact shear stiffness calculated based on specific methodology used in study:

$$K_T = \frac{k_s^{[A]} k_s^{[B]}}{k_s^{[A]} + k_s^{[B]}} \tag{4}$$

where, $k_n^{[A]}, k_n^{[B]}, k_s^{[A]}, k_s^{[B]}$ are the normal and shear stiffnesses.

The updated shear contact force is calculated as:

$$\vec{F}_T \leftarrow \vec{F}_T + \delta\vec{F}_T \leq \mu\,\vec{F}_N \tag{5}$$

where, μ is the coefficient of friction.

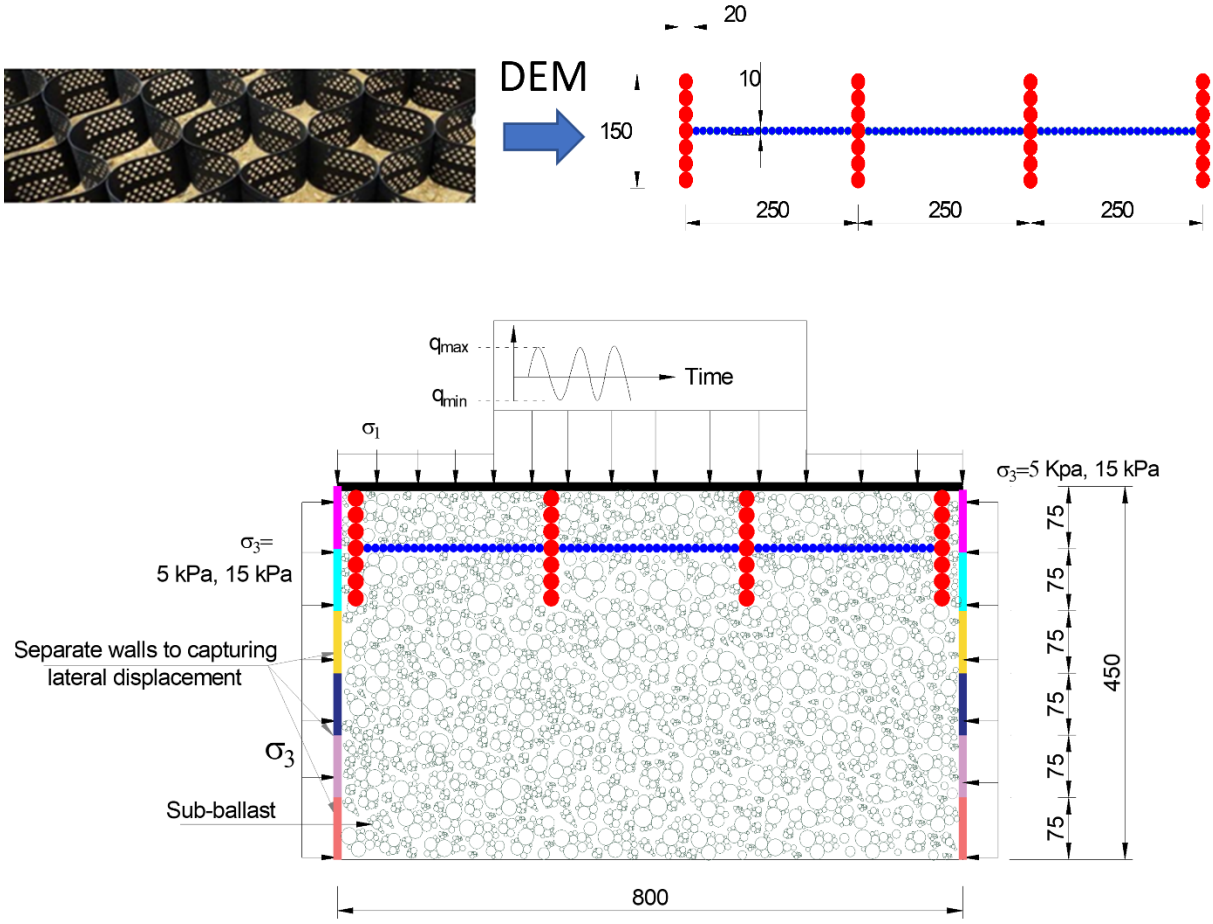

Figure 2. Modelling of geocell and large-scale TPSA in DEM

Micromechanical parameters used for the DEM

Modeling geocells in three dimensions can be computationally demanding due to their intricate 3D honeycomb structure. To overcome this challenge, a simplified two-dimensional plane strain representation was employed in this study, enabling the DEM model to yield results efficiently. The geocell's 3D structure was approximated using bonded particles arranged in connected strings, with vertical and horizontal panels constructed using 20mm and 10mm diameter balls, respectively. This approach effectively captured the confinement effect of the geocell by confining particles within the simulated pockets. Micromechanical parameters for the geocell were determined through DEM simulations of tensile and bending tests, with the resulting force-strain responses compared to experimental data for calibration purposes. The parallel bond stiffness in the DEM model was fine-tuned to match laboratory tensile test results. The specific input parameters utilized in the model can be found in the provided Table 1.

Table 1. Micro-mechanical parameters used for DEM model

Parameter	Geocell	Capping
Particle density (kN/m^3)	9.5	21
Coefficient of friction	0.45	0.72
Contact normal stiffness, k_n (N/m)	6.51×10^6	2.56×10^8
Contact shear stiffness, k_s (N/m)	6.51×10^6	2.56×10^8
Parameter of contact bond normal strength, ϕ_n(kN)	43.2	5.36×10^9
Parameter of contact bond shear strength, ϕ_s (kN)	43.2	8.53×10^9
Parallel bond radius multiplier, r_p	0.5	0.5
Parallel bond normal stiffness, k_{np} (kPa/m)	4.86×10^7	
Parallel bond shear stiffness, k_{sp} (kPa/m)	4.86×10^7	
Parallel bond normal strength, σ_{np} (MPa)	352	
Parallel bond shear strength, σ_{sp} (MPa)	352	

RESULTS AND DISCUSSION

Vertical and lateral displacements

Figure 3 presents a comparison between the average accumulated settlement obtained from DEM simulations and experimental results at different load cycles. The DEM analysis showed reasonable agreement with the experimental data for various frequencies and loading cycles. Results indicated that settlement increased with higher frequencies and that geocell-reinforced capping exhibited less settlement compared to the unreinforced assembly. This can be attributed to the geocell's confining pressure, reducing capping deformation. When capping aggregates were compacted over the geocell, they formed a stiff mechanical structure, acting as a presumably non-displacement boundary and resulting in reduced settlement. Initially, settlement accelerated due to particle compression and rearrangement, followed by a slower rate of increase in subsequent load cycles. At very high load cycles, settlement reached an approximately constant value. Additionally, the lateral deformation of capping, parallel to the sleeper, was compared between DEM modeling and experiments, showing a good level of agreement. The geocell effectively reduced lateral deformation by restraining the capping and creating a stiffened zone. Despite limitations arising from the plane strain assumption, the 2D DEM model successfully captured the load-deformation behavior of geocell-stabilized capping.

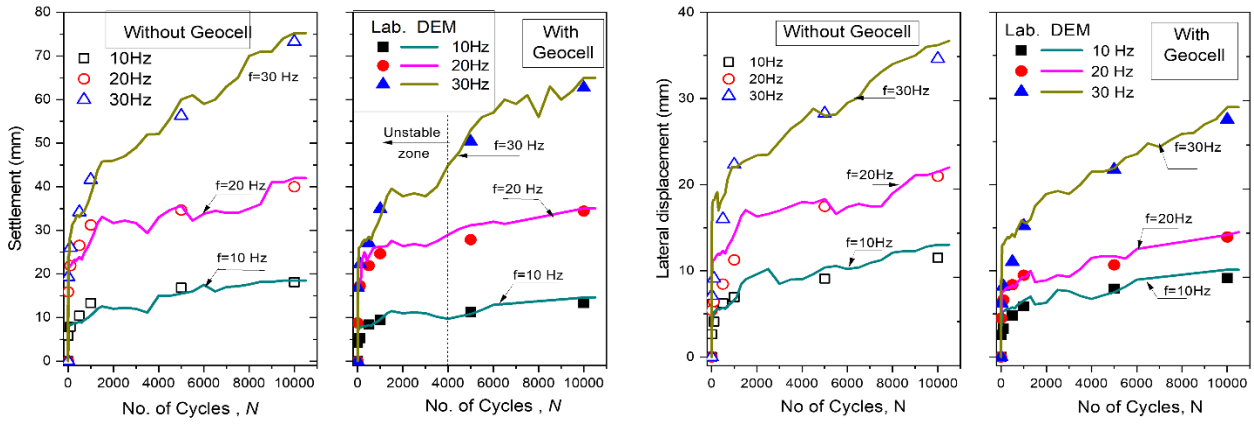

Figure 3. Comparison between the laboratory tests and DEM simulation: (a) vertical settlement; (b) lateral displacement (Source: Ngo et al. 2016 – with permission from ASCE)

Contact force distributions

Figure 4a illustrates the distribution of contact forces in an unreinforced capping subjected to cyclic loading at a f= 20 Hz and a settlement, S= 5 mm. On the other hand, Figures 4b-d present the results of geocell-reinforced capping specimens. Thicker lines represent higher forces, and only contact forces exceeding the mean forces of the specimen are shown. As settlement increases, both the total number and maximum magnitude of contact forces rise. For geocell-reinforced capping, the number of contacts increases from 60,252 at S=5mm to 78,252 and 83,521 at S=15, 20mm, respectively. This indicates enhanced particle interaction and contact forces within the geocell-reinforced capping. The contact force distributions visually illustrate the influence of settlement on the distribution and magnitude of contact forces in the geocell-reinforced system. These findings provide insights into the behavior and mechanics of geocell-reinforced capping under cyclic loading conditions, highlighting the effectiveness of geocells in enhancing the structural response and stability of the capping layer.

As settlement increases, the maximum contact forces in the geocell-reinforced capping also increase, reaching values of 745 N, 857 N, and 946 N for S = 5, 15 and 20mm, respectively. Compared to the unreinforced capping, the reinforced assemblies exhibit a higher number of contact forces within the geocell regions, indicating the beneficial confinement effect of the geocell on the capping material. The results also demonstrate the activation of tensile forces within the geocells, shown in red, which become more prominent with increasing settlement. These findings provide valuable insights into the behavior and performance of geocell-reinforced capping under cyclic loading conditions.

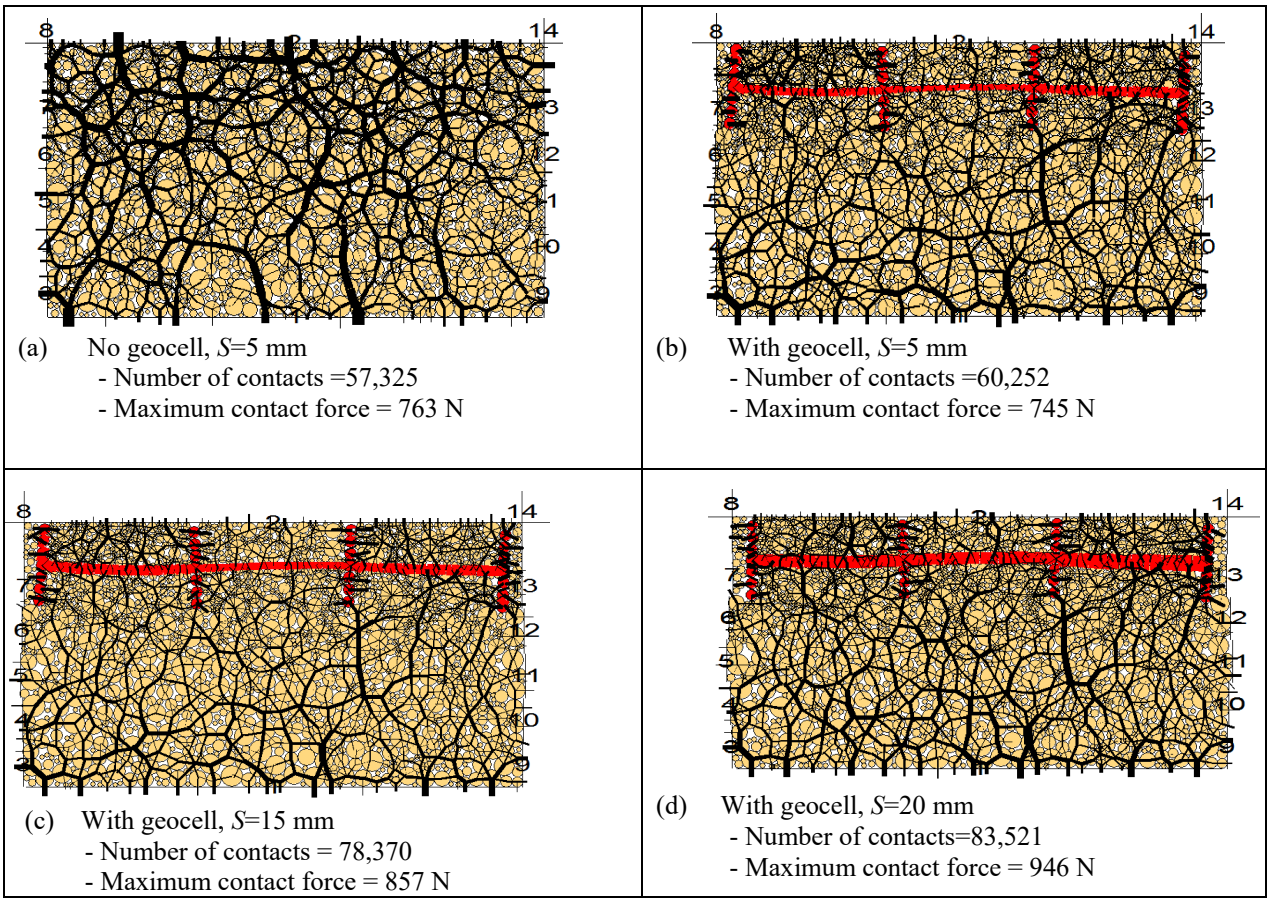

Figure 4. Changes of contact forces with the settlement: (a) unreinforced, *S*=5 mm; (b) *S*=5mm (reinforced); (c)*S*=15mm (reinforced); (d) *S*=20mm (reinforced) (Source: Ngo et al. 2016- with permission from ASCE)

Variations of Contact Normal and Shear Forces

Figure 5 depicts the changes in normal and shear contact forces with depth for both types of capping layers after 10,000 cycles. The geocell-reinforced capping demonstrates elevated contact forces within the geocell zone compared to the unreinforced specimens. However, below the geocell zone, the average contact forces gradually decrease with increasing depth and eventually reach nearly constant values near the bottom of the assembly. It is important to note that the authors simplified the micro-mechanical analysis to maintain simplicity and brevity in this paper. As a result, more detailed DEM analyses capturing aspects like fabric anisotropy and changing angularity with a large number of cycles were not reported. It is noted that while a 2D model might not fully replicate the intricacies of a true 3D scenario, it can still provide valuable insights into the mechanics and behavior of geocell applications. By carefully selecting appropriate boundary conditions, considering material properties, and incorporating aspects of geocell-ballast interaction, a 2D model can offer valuable approximations of the contact force distribution and load-deformation characteristics introduced by geocells.

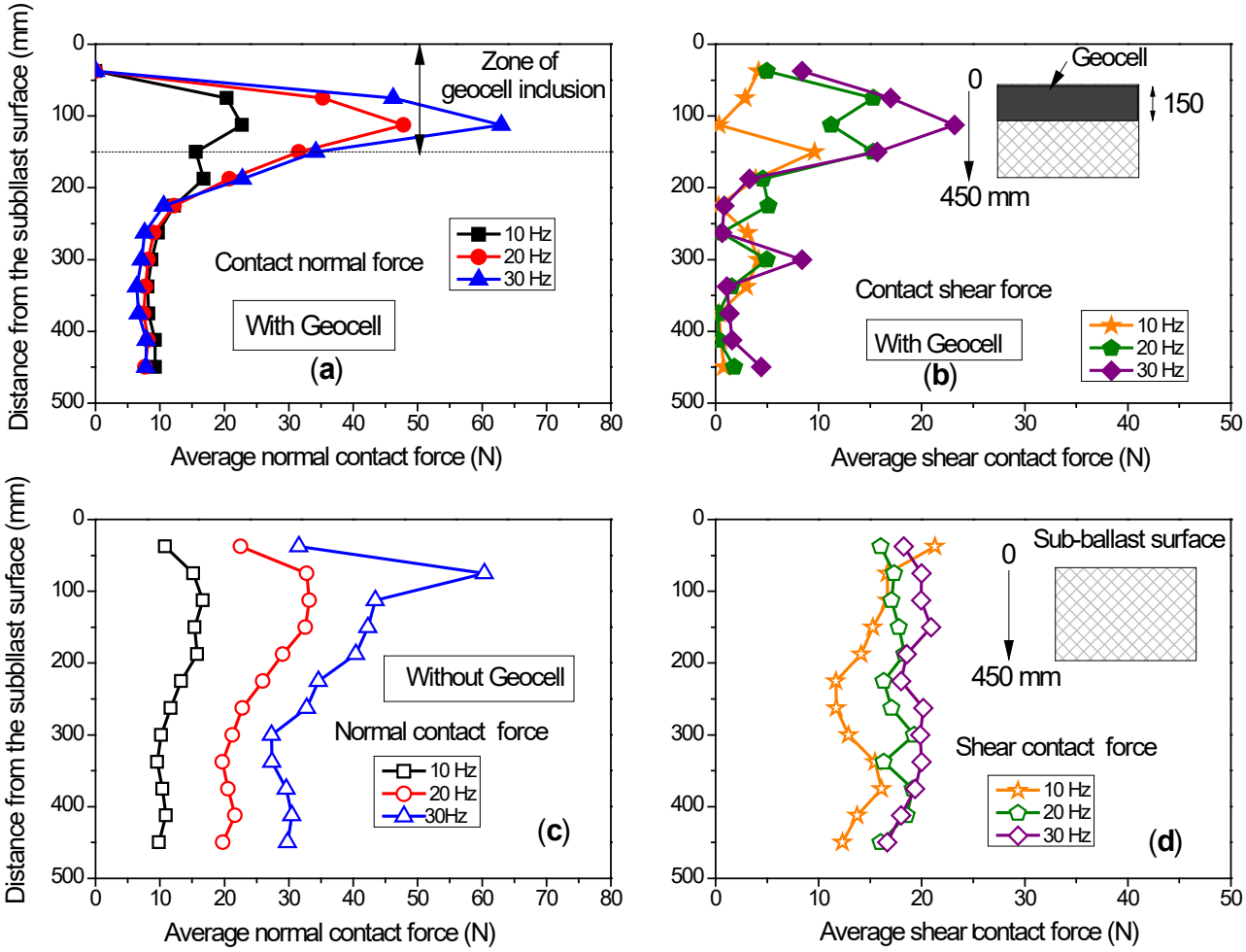

Figure 5. Distribution of contact forces: (a) & (b) - with geocell; (c) & (d) - without geocell (Source: Ngo et al. 2016- with permission from ASCE)

CONCLUSION

Cyclic tests were performed on capping materials, with and without geocell reinforcement. The DEM analysis was calibrated and compared to the test results, allowing the identification of input parameters for simulating the capping and geocell behavior. These parameters were calibrated earlier and adopted to model cyclic tests on capping aggregates under different frequencies.

The experimental data for settlement and lateral displacement closely matched those obtained from the DEM simulations for a specific frequency. The inclusion of a geocell in the capping resulted in reduced deformation compared to the unreinforced sample, thanks to the confinement effect of the geocell. These findings demonstrated that the DEM successfully captured the load-deformation characteristics of the geocell-reinforced capping assembly.

The examination of contact force distributions in geocell-reinforced capping demonstrated an increase in the maximum contact force with progressive deformation. The contact forces, both normal and shear, between particles within the capping were examined at different depths. The magnitudes of these forces were notably higher within the geocell zone compared to other regions. However, as depth increased below the geocell, the average contact forces decreased and eventually stabilized at near-constant values towards the bottom of the granular assembly.

ACKNOWLEDGEMENTS

The research conducted in this study was supported by funding from the ARC Discovery Project (DP220102862). The authors acknowledge for the valuable collaboration given by Transport for NSW, Sydney Trains, SMEC, Australian Rail Track Corporation (ARTC), and other industry partners. The authors also extend their appreciation to ASCE for granting permission to reproduce certain research outcomes in this paper.

REFERENCES

Astaraki, F., Esmaeili, M. and Reza Roozbini, M., 2022. Influence of geocell on bearing capacity and settlement of railway embankments: an experimental study. *Geomech. Geoengin.*, 17(2), 630-646.

Banerjee, L., Chawla, S. and Dash, S.K., 2020. Application of geocell reinforced coal mine overburden waste as subballast in railway tracks on weak subgrade. *Constr. Build. Mater.*, 265, 120774.

Bathurst and Raymond (1987). Geogrid reinforcement of ballasted track. *Transp. Res. Rec*. 1153: 8-14.

Biabani, M. M., B. Indraratna and N. T. Ngo (2016). Modelling of geocell-reinforced subballast subjected to cyclic loading. *Geotext. Geomembr.* 44(4): 489-503.

Biabani, M. M., N. T. Ngo and B. Indraratna (2016). Performance evaluation of railway subballast stabilised with geocell based on pull-out testing. *Geotext. Geomembr.* 44(4): 579-591.

Bian, X., W. Li, Y. Qian and E. Tutumluer (2020). Analysing the effect of principal stress rotation on railway track settlement by discrete element method. *Géotechnique*. 70(9): 803–821.

Bolton, M. D., Y. Nakata and Y. P. Cheng (2008). Micro- and macro-mechanical behaviour of DEM crushable materials. *Géotechnique*. 58(6): 471–480.

Brown, S. F., J. Kwan and N. H. Thom (2007). Identifying the key parameters that influence geogrid reinforcement of railway ballast. *Geotext. Geomembr.* 25(6): 326-335.

Cui, L. and C. O'Sullivan (2006). Exploring the macro- and micro-scale response of an idealised granular material in the direct shear apparatus. *Géotechnique*. 56(7): 455-468.

Cundall, P. A. and O. D. L. Strack (1979). A discrete numerical model for granular assemblies. *Géotechnique*. 29(1): 47-65.

Esveld, C. (2014). Modern railway track, MRT Press, The Netherlands.

Indraratna, Biabani and Nimbalkar (2015). Behavior of Geocell-Reinforced Subballast Subjected to Cyclic Loading in Plane-Strain Condition. *J Geotech Geoenviron*. 141(1): 04014081.

Indraratna, B. and T. Ngo (2018). Ballast Railroad Design: Smart-Uow Approach, CRC Press.

Indraratna, B., Q. Sun, N. T. Ngo and C. Rujikiatkamjorn (2017). Current research into ballasted rail tracks: model tests and their practical implications. *Aust. J. Struct. Eng.* 1-17.

Leshchinsky, B. and H. I. Ling (2013). Numerical modeling of behavior of railway ballasted structure with geocell confinement. *Geotext. Geomembr.* 36: 33-43.

Luo, Z., C. Zhao, X. Bian and Y. Chen (2023). Discrete element analysis of geogrid-stabilized ballasted tracks under high-speed train moving loads. *Comput Geotech*. 159.

McDowell, G. R. and H. Li (2016). Discrete element modelling of scaled railway ballast under triaxial conditions. *Granul. Matter*. 18(3): 66.

Ngo, N. T., B. Indraratna, C. Rujikiatkamjorn and M. M. Biabani (2016). Experimental and Discrete Element Modeling of Geocell-Stabilized Subballast Subjected to Cyclic Loading. *J Geotech Geoenviron*. 142(4): 04015100.

Selig, E. and Waters (1994). Track geotechnology and substructure management, Thomas Telford, London.

Tran, K. M., H. H. Bui, M. Sánchez and J. Kodikara (2020). A DEM approach to study desiccation processes in slurry soils. *Comput Geotech*. 120: 103448.

Tran, V. D. H., M. A. Meguid and L. E. Chouinard (2013). A finite–discrete element framework for the 3D modeling of geogrid–soil interaction under pullout loading conditions. *Geotext. Geomembr*. 37: 1-9.

Tutumluer, E., Huang and X. Bian (2012). Geogrid-Aggregate Interlock Mechanism Investigated through Aggregate Imaging-Based Discrete Element Modeling Approach. *Int. J. Geomech*. 12(4): 391-398.

Zhang, X., C. Zhao and W. Zhai (2019). Importance of load frequency in applying cyclic loads to investigate ballast deformation under high-speed train loads. *Soil Dyn. Earthq. Eng*. 120: 28-38.